Collagen-Electrohydrodynamic Hierarchical Lithography for Biomimetic Photonic Micro-Nanomaterials

McCarthy, Emma; Thomas, Jarrod; Oppenheimer, Roni; Rickard, Jonathan J. S.; Goldberg, Pola

DOI:
10.1002/smll.202402565

NANO · MICRO small
www.small-journal.com

Collagen-Electrohydrodynamic Hierarchical Lithography for Biomimetic Photonic Micro-Nanomaterials

*Emma McCarthy, Jarrod Thomas, Roni Oppenheimer, Jonathan J. S. Rickard, and Pola Goldberg**

Biologically engineered nanomaterials give rise to unique and intriguing properties, which are not available in nature. The full-realization of such has been hindered by the lack of robust and straightforward techniques to produce the required architectures. Here a new bottomup bionano-engineering route is developed to construct nanomaterials using a guided assembly of collagen building blocks, establishing a lithographic process for three-dimensional collagen-based hierarchical micronano-architectures. By introducing optimized hybrid electro-hydrodynamic micronano-lithography exploiting collagen molecules as biological building blocks to self-assemble into a complex variety of structures, quasi-ordered mimics of metamaterials-like are constructed. The tailor-designed engineered apparatus generates the underlying substrates with vertical orientation of collagen at controlled speeds. Templating these hierarchical structures into inorganic materials allows the replication of their network into periodic metal micronano-assemblies. These generate substrates with interesting optical properties, suggesting that size-and-orientation dependent nanofilaments with varying degree of lateral order yield distinctly coloured structures with characteristic optical spectra correlated with observed colours, which varying diameters and interspacing, are attributable to coherent scattering by different periodicity of each fibrous micronano-structure. The artificial mimics display similar optical characteristics to the natural butterfly wing's structure, known to exhibit extraordinary electromagnetic properties, driving future applications in cloaking, super-lenses, photovoltaics and photodetectors.

1. Introduction

Patterns, ranging from macro to nano levels, are an integral part of our everyday lives, and they may be found nearly anywhere, in nature, in art, in mathematics, in imaging, and in technology. Micronano-structured films are often used in sensors or in the semiconductor industry for the fabrication of micro and nanoelectronic devices. The patterns found in nature, where properties are largely determined by the surface energy as well as the surface structure, are particularly intriguing. Intricate, hierarchical structures found in certain living creatures are responsible for the fascinating properties and features such as iridescence, camouflaging, or improved fluidics while spanning many length scales. For instance, self-cleaning leaves are based on patterns comprised of microscopic wax crystals whilst periodic arrays in butterfly wings lead to colorful optical properties and their iridescent surfaces help them to elude potential predators.

Butterfly wings, due to their 3D micronano-architectured layers known to exhibit unique structural colors,[1] circular polarization,[2] and dynamic optical changes.[3] The hierarchical unique photonic, multilayer, or helicoidal structure assemblies of the wing scales play a critical role in the formation of structural colors due to the interaction of light with 2D or 3D periodic sub-micro architectures. A prominent example is the angular blue/greenish color change of the *Morpho Didius* (**Figure 1a**), generated by the topography of the wings and their photonic crystal structure. Davis et al. have shown that many butterflies possess scales with

E. McCarthy, J. Thomas, R. Oppenheimer, J. J. S. Rickard, P. Goldberg
School of Chemical Engineering, Advanced Nanomaterials Structures and Applications Laboratories, College of Engineering and Physical Sciences
University of Birmingham
Edgbaston, Birmingham B15 2TT, UK
E-mail: goldberp@bham.ac.uk

The ORCID identification number(s) for the author(s) of this article can be found under https://doi.org/10.1002/smll.202402565

DOI: 10.1002/smll.202402565

E. McCarthy
CMR Surgical
Business Park, Milton Road, Cambridge CB24 9NG, UK
J. J. S. Rickard
Department of Physics, Cavendish Laboratory
University of Cambridge
JJ Thomson Avenue, Cambridge CB3 0HE, UK
P. Goldberg
Healthcare Technologies Institute
Institute of Translational Medicine
Mindelsohn Way, Birmingham B15 2TH, UK

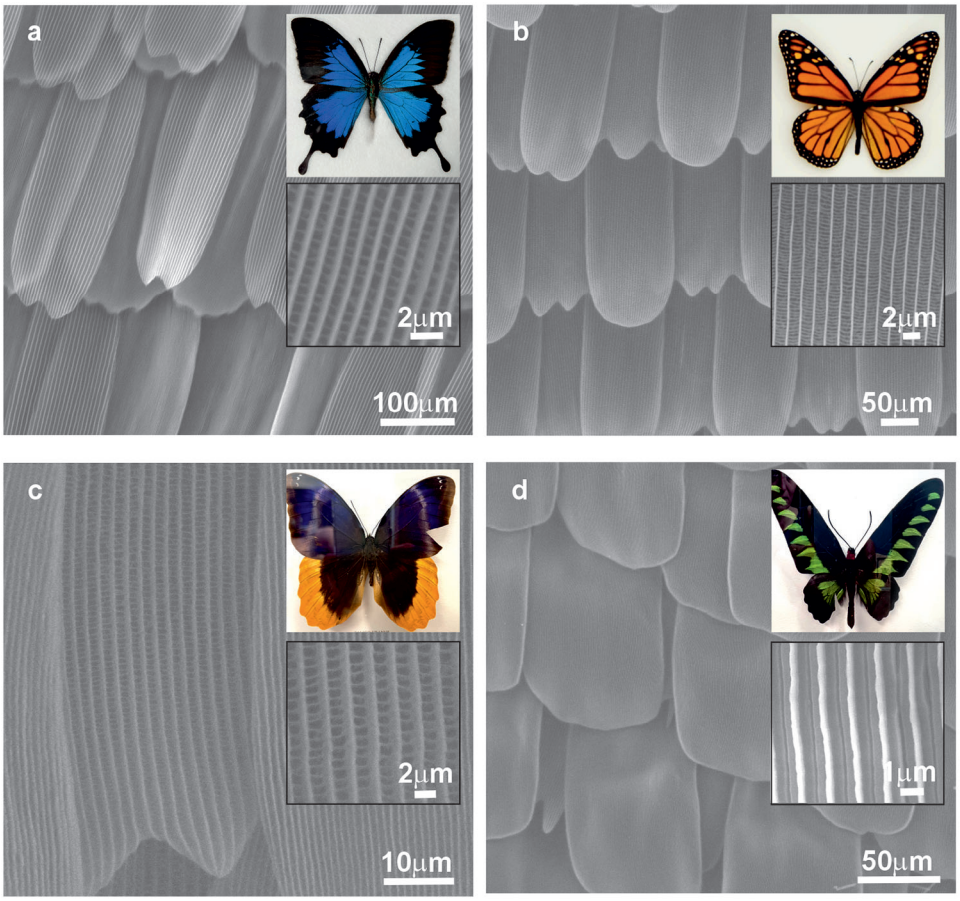

Figure 1. SEM images with zoom-in micrographs (inset, bottom) and photographs (inset, top) of the hierarchical micro- and nanostructures of the a) *Morpho*, b) *Danaus Plexppusi (Monarch)*, c) *Caligo Uranus* and d) *Brookiana* butterfly wings overviewing the various periodic arrangement and overlapping micro-scales on the wings and fine lamella-stacking nano-stripes on the scales.

an upper lamina perforated by quasi-periodic holes with a considerable variation in shape and size, including hexagonal, chevron-shaped, or rectangular holes.[4] Yan et al. have systematically studied a range of butterfly wing scales and based on the morphological characterization and 3D schematic models, established theoretical optical simulations.[5] Albeit only several representative prototype models of butterflies, e.g., *Papilio Nireus* and *Paris*, *Troides Helena* were chosen, the study has provided an important generic classification of microstructures sharing common characteristics. These include periodic inverse ridges parallel to the longitudinal axis of the scale combined with a basal substrate, consisting of two chitin layers and a chitin–air layer between them, forming a Bragg reflector[6] with further air space with disordered columnar pillars as upholders above the substrate. Subdissimilarities are found to be based on sets of hole arrays (with varying dimensions and distributions), which can be hexagonal in the host lamina, forming a 2D photonic crystal or rectangular nano-hole arrays in double or triple-row pattern. These hierarchical arrays regulate the optical reflection and absorption characteristics determined by the underlying 3D micronano architectures.

Inspired by nature's staggering designs in the past decades, science and technology have been experiencing the germination of new methods and fabrication technologies for micro and nanopatterning, which are essential for enabling a variety of advanced applications. The control of patterns on submicrometer lateral length scales is of considerable technological interest and is especially relevant for tailoring the properties of novel functional materials. A variety of bottom–up, using molecular building components to achieve structures and networks via chemical self-assembly and top–down, encompassing the fabrication of materials with a predesigned functionality, techniques for patterning polymer resists have been continuously evolving. The most prominent examples include photolithography, laser writing, electron beam lithography, soft lithography imprinting, self-assembly of block copolymers, molding or embossing-based techniques, and holographic patterning.[7–12] Hitherto, however, most of the existing strategies for patterning polymers have revealed limitations in certain aspects. Among the difficulties are those related to resolution, position control, physical limits, production of hazardous by-products during the fabrication process, versatility, and reproducibility. While most micro-to-nano lithographic techniques utilize resists of macromolecular nature, the extension toward additional materials, such as biologically inspired systems, is of major importance. These could enable invaluable surface functionalities that cannot be accomplished with polymers alone. Moreover, for many applications, such as metamaterials, it is desirable to control the spatial arrangement of more than one component and although stacks consisting of

three or four functional layers have been reported, true 3D metamaterials are yet to be accomplished. With traditional methods the process requires iterative, multistep, procedures, rendering the patterning methods intricate and less scalable. Novel, cost-effective lithographic processes are needed to enable straightforward patterning in a controlled manner on multiple scales, which will also be suitable for a broad range of materials. Development of these is essential for the successful future large-scale fabrication of advanced micro and nano-devices.

Concurrently, the emerging interdisciplinary field of synthetic biology, combining unconventional approaches from biology, physics, and engineering, has recently yielded the construction of novel biomolecular components, networks, and pathways.[13,14] This has demonstrated the possibility of exploiting and rewiring bio-organisms to establish unique properties, which are not easily achievable using conventional components and techniques alone. Biological and molecular building blocks and their controlled assembly thus, pose as excellent constituents for the development of nano-engineered systems with desired biomimetic, bio-metamaterial, chiroptical, or photonic properties. Such systems, being driven toward energetically more favorable configurations with increased molecular sensitivity and recognition, render the biologically inspired materials as ideal building blocks for micro and nanoscale molecular structuring. By exploiting synthetic biology origin nature's building blocks via collagen-based micro- and nanostructuring can enable a straightforward and cost-effective formation of nanostructures with two to three characteristic lateral dimensions to generate lithographically defined architectures.

Within these, controllably assembled bionano-structures based on the collagen chassis could offer greater versatility, enabling the arrangement of micro-nanometric components with characteristic length scales ranging from a few to several hundreds of nanometers and thus, tuning the dimensions as well as properties. Collagen is a family of 28 proteins, which share the same general repeating amino acid structure, i.e., Gly-X-Y, where X and Y typically represent proline and hydroxyproline.[15] Collagen fibrils are 300 nm in length yet, can be assembled to form fibers with diameters smaller than 15 nm their[16–19] assembly can easily be modified via small environmental and chemical modifications. The repeating structure and small size of the glycine means that the collagen molecule naturally forms a helical structure in solution. In the right conditions, these helices can assemble to form nano-fibrils and then fibers (on the μm scale). The process of collagen assembly is physically or chemically driven and can be influenced by a broad range of variables, including the presence of ions that interact with the forming fibers,[20] temperature,[21] or the presence of molecules, which mediate fiber nucleation or organization. The broad possibilities that are open for structural modification by manipulating collagen assembly are best illustrated through the enormous differences between tissues, which are principally formed from collagen. For instance, the cornea is transparent and compliant, because of the highly conserved assembly of collagen I fibers, i.e., 15 nm average diameter, in repeating layers acting as an optical grating.[22] Bone is also formed from collagen type I with dimensions of 50–200 nm, which is deposited parallel to the main loading axis, providing optimal tensile properties and mineralization to provide resistance in compression. To date, it has been demonstrated that it is possible to shape collagen assembly processes by utilizing cations,[23] applying compaction,[24] exploiting cell populations,[25] and the previously fibrillized collagen has been used as a support material in a range of biomedical applications.[26] We have also demonstrated the use of the combination of the electric field and the hydrodynamics by patterning dielectric materials, conductive and crystalline materials, and superapolar lotus-to-rose hierarchical surfaces, with the controllable alignment of the internal nano-morphologies.[27–32] However, there have been no attempts to guide the assembly of collagen fibers particularly, as template structures for new metamaterials or biomimetics and particularly, by providing topographical micropatterned cues, which result in hierarchical micro-nanostructures, new optical properties as well as biophonic effects, such as seen in butterfly wings (Figure 1). The flexibility and high aspect ratio for the functionality of collagen, combined with its availability for scalable production, render it ideal from both a fundamental science and application standpoint.

Herein, we have developed a novel lithographic route of exploiting collagen (type I) as bottom–up building blocks for diverse 3D bionanomaterial structuring, inaccessible via conventional patterning techniques or inorganic chemistry. Collagen-based patterning enables a straightforward and cost-effective formation of nanostructures with two to three characteristic lateral dimensions via the synthetic biology origin to generate lithographically defined architectures.

Particularly, by exploiting the filamentous nature of collagen to construct 3D quasi-ordered biomimetics, we have introduced an optimized hybrid Electro–Hydro dynamic micronano lithography combined with harnessing the capacity of Collagen (EHCgen) molecules to self-assemble into a complex variety of structures as a templating intermediate to fabricate hierarchical architectures (**Figure 2**), whilst enabling structural tuneability and flexibility overcoming the challenges of complete structural replication. In this EHCgen lithographic mode collagen is assembled via several programmed interactions, to produce 3D biomimetic structures and potential bionanomaterials, which can integrate technologies across several orders of magnitude using a high throughput process. In a simplified analogy, the modular collagen (exploited for its intrinsically hierarchical structure) building molecules, like LEGO blocks, fit together in a distinctive manner and can subsequently be used to design complex architectures in terms of structure and property. Our approach, therefore, allows the development of 3D nano-lithographic structuring using collagen type I as a building block to enable the directed assembly of biomaterials used to fabricate hierarchical micro- and nanoarchitectures (Figure 2). Subsequent to the proof-of-concept of scalable production of micronano-structured surfaces, we have identified how variations in surfaces can allow the tuning of micro and nanostructures and the resulting optical properties.

This unconventional lithographic route enables the arrangement of components with characteristic length scales ranging from nanometers to micrometers and controls over variation of the order, periodicity, and dielectric contrast. EHCgen lithography could further allow the construction of a virtually unlimited range of micro to nano-network structures of any desired morphology. The concept of changing the bionanomaterial's shape and spacing of internal structures opens the door to transforming light in many ways. This includes, for instance, the reverse

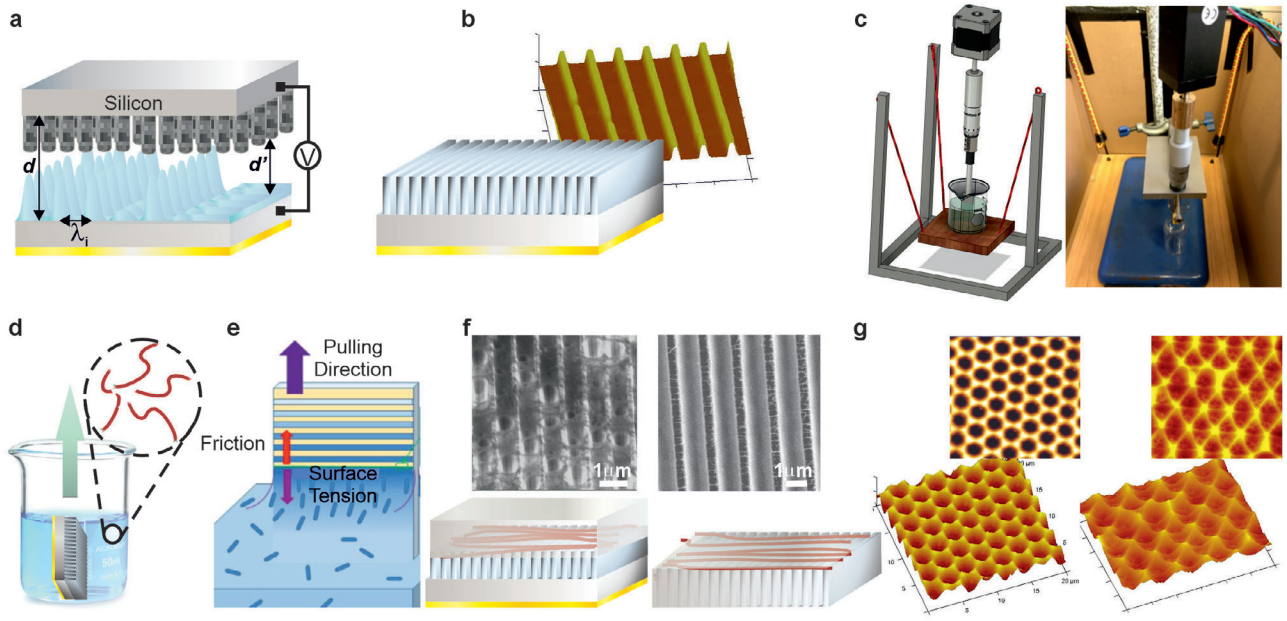

Figure 2. a) Schematic of capacitor device during the EHMN process under a laterally heterogeneous electric field. A structured upper electrode creates a heterogeneous force field focusing the instability toward the protruding structures. The initial capillary plugs span the substrate and protruding lines, leading to an increasing coalescence and subsequently, b) a positive replica of the master pattern is transferred into the polymer. In unstructured regions, the film remains stable on a much longer timer scale. (b, inset) AFM 3D image of the pattern replication of a line grating after the removal of the master electrode. c) A controllable evaporative deposition rig consists of a clamp stand placed atop a wooden block suspended via bungee cords within an enclosure. The micrometer allows micro-adjustments of the speed within a few microns. d). The EHMN patterned substrate, fixed to the non-rotating head of the micrometer and connected to the step motor, is placed within the templating collagen solution in a beaker, connected to the Gerbot GUI interface coded via a Raspberry Pi combined with a Gertbot hat used to control the pulling speed. A voltmeter is used to drive the motion of the micromotor, where the power supply allows the spindle to non-rotating head to controllably withdraw the fixed substrate from the solution along the *y*-axis. e) This yields the vertically aligned collagen f) perpendicular to the underlying EHMN substrate grating, which can also be embedded in epoxy resin and upon scaffold removal yield the free-standing inverted 3D EHCgen (bottom right) hierarchical micro- and nanoarchitecture, subsequently g) gold-plated via electrodeposition and sputter-coating.

Doppler effect, super lensing, cloaking, and camouflaging devices. The fabricated 3D collagen architectures can be further exploited as guiding scaffolds for patterning metals or ceramics to create novel photonic or advanced miniaturized devices. For instance, transferring the periodic replicas into nanostructured functional systems, via electrochemically grown materials from underlying substrates and subsequent selective degradation of the sacrificial collagen template via matrix metalloproteinases, could deliver freestanding 3D architectures made from new materials, exhibiting interesting optical metamaterial-like characteristics. Importantly, collagen type I is a ubiquitous molecule in mammalian tissues, and is widely available, which further lends itself to scaling up of the overall lithographic process.

2. Results and Discussion

2.1. Fabrication of Electrohydrodynamically Patterned Topographic Underlying Substrates

First, we have designed guiding micro-substrates to act as anchors for the collagen, yielding tailor-designed large-area arrays with tuneable placement and spacing between the nanostructures. Commencing with the electro hydrodynamic micro nano (EHMN) patterning to fabricate the underlying primary substrates, where we harness the initial film instability to replicate a wide range of patterns with high-fidelity and micro to nanometric lateral length scales. The developed EHMN setup included a capacitor-like assembled device, within which a thin polymer nano-film is deposited on the bottom electrode, as opposed to the topographically structured upper electrode. When annealed above the glass transition temperature, the nano-film begins to flow as a viscous liquid. Consequently, applying an electric field normal to the initially homogeneous interface yields the destabilizing interfacial electrostatic pressure. The latter overcomes the stabilization of the Laplace pressure and couples to the capillary wave spectrum, amplifying surface instabilities with a characteristic wavelength. For an applied electric field, the topographic pattern of the top electrode constitutes an equipotential surface, and the instability is focused in the direction of the highest electric field (Figure 2a). Since, the electrostatic pressure is much stronger for smaller inter-electrode distances, pattern replication of topographically structured upper electrode proceeds at a rapid time scale. The instability is guided toward the protruding patterns of the top mask, where the liquified polymer is drawn toward these protrusions (Figure S1, Supporting Information), forming a positive replica (Figure 2b; Figure S2, Supporting Information). A successful pattern replication requires harmonizing the length scale of the master pattern and the instability characteristic wavelength. Importantly, EHMN enables cost-effective large-area fabrication of micro nanostructured

platforms with an inherent capability to directly pattern any material of choice with tuneable dimensions. This, in turn, enables fabricating tailor-designed underlying substrates with various surface energy, which modifies how collagen assembles onto the surface, laying the platform for the successive structural assembly across several orders of magnitude via a single process.

2.2. Optimization of the Collagen Fibrils Assembly

The process of collagen assembly is physically driven and can be influenced by a broad range of variables, including the presence of ions that interact with the forming fibers, temperature, or the presence of molecules, which mediate fiber nucleation or organization. To establish assembly conditions for the design of collagen-based micronano-structured platforms, we have optimized the thermally driven and pH-dependent process to modulate the collagen assembly, with native fibrils typically forming within ranges of 5.0< pH<8.5 and 15–37 °C.[33,34] Whilst the pH of the solution in which collagen is dispersed affects the stability of the fibrils, influencing both the D-spacing and fibril diameter,[34,35] temperature affects the hydrophobic interactions, which influence the kinetics of fibril formation alongside the pH.[36] Therefore, building upon collagen's ability to assemble to produce the modified collagen constructs with improved assembly characteristics, we have established optimal assembly-related parameters (Figures S3 and S4, Supporting Information). These subsequently allowed us to control the deposition, assembly, and lithographic process as well as inform the modeling of the structures for novel optical properties and metamaterial-like performance. The parameters for the concentration, pH, and temperature[37] were found to be (1.2–1.6 ± 0.75–0.93 mg mL^{-1}), (6.6–7.2 ± 0.9–1.5) and (18–36 °C), respectively. The established and chosen collagen I fibrils for the subsequent EHCGen patterning had dimeters of 9–16 ± 1.2–3 nm, 50–300 nm lengths, and D-spacing of 63 nm, on average. These findings are in correspondence with studies of Li et al. and Harris et al.,[34,38] who have shown that a pH of 2.5 prevents collagen from aggregating whilst, at pH 7, it aggregates to display characteristic D-spacing with aligned clustering. At higher pH, fibrils become uniform and form a matrix, with pH>6.6 enabling fibrils of 85 nm in diameter. Although the rate at which fibrils form at 6.6<pH<8.0 varies, the final diameter and D-spacing across this range are consistent ≈200 nm[34,38] and 62 nm, respectively.[34] Overall, collagen at higher pH is more compact regardless of ionic strength[36] due to an increased formation of net electrostatic interactions between charged side groups, increasing attraction and yielding tighter packing assemblies.

2.3. Ordering Collagen on the EHMN Substrates via Controllable Evaporative Deposition

Subsequently, we have designed an in-house rig for a controllable evaporative deposition consisting of an automated micrometer withdrawal system controlled through a Raspberry Pi and configured with a Gertbot GUI, which allows for the drawing speeds (range: 01.47–148.50 µm min^{-1}), required for ordering collagen on substrates through adherence of the fibril onto the lithographically defined underlying features (Figure 2c). This, in turn, provided a tuneable and facile approach for pattern collagen-based desired nanomaterials, allowing the production of hierarchical 3D structured arrays. When the EHMN substrates are vertically pulled, the fastest rate of evaporation is at the air–liquid–solid contact line, resulting in the localized deposition of collagen fibers on the substrate (Figure 2d). The micrometer allows micro-adjustments of the speed within a few microns. Two factors play an important role in this lithographic process, the local induction of liquid-crystal phase transitions and the presence of competing interfacial forces, of surface tension versus friction (Figure 2e), both acting at the meniscus, which determine the collagen orientation, material flux and the higher-order organization. Through the interplay of these factors, we create a range of lithographically defined micronano-structured surfaces made of gold, which have the architecture of optical metamaterials (Figure 2f,g; Figure S2, Supporting Information).

Collagen fibers were guided using underlying topographical microcues. Interestingly, a preferential orientation perpendicular to the underlying micro-grating on the substrate has been consistently observed irrespective of the direction of the grating (Figures 2f, 3, 4), contrasting the previous study by Brudzinski et al., who used patterned titanium surfaces to orientate both cells and collagen in parallel to grooves.[39] Immersion of the EHMN substrates in collagen solution which excluded the controllable evaporative deposition step, yielded a low degree of parallel fibrils coalignment and did not lead to the perpendicular orientation. To determine the optimal topographical parameters for collagen micronano structuring, we have systematically evaluated the degree of collagen ordering (<concentration> = 1.0 ± 0.2 mg mL^{-1}) for a range of ridge-to-groove (RTG) ratios. It was found that whilst surfaces with an RTG ratio of 0.7 did not yield collagen alignment, a preferential assembly of collagen in a perpendicular direction on substrates with 1.45<RTG<1.56 ratio was consistently observed. Subsequently, we have established the degree of perpendicular assembly of collagen by measuring the angle between the ridge edge and the fibril. All surfaces which produced vertical collagen orientation within 10° of each other were taken into consideration (Figure 3a–c), out of which, two guiding micro-substrates of RTG 1.4 and 1.5 exhibited a statistically significant degree of organization (Figure 3b,c). To ensure that alignment was not concentration dependent, w/v of 0.5, 1, 1.25, 1.5, and 1.75 mg mL^{-1} of collagen was deposited onto patterned substrates and analyzed via electron microscopy imaging. To quantify collagen degree of order at different concentrations, the angle between the ridge edge and collagen fibril was measured. All concentrations exhibited a significant perpendicular alignment to the surface under-structure, however, there was a higher degree of consistency between concentrations of collagen deposited onto the micro-patterned surface using an RTG ratio of 1.5, which yielded the highest percentage of perpendicularly assembled fibrils with the lowest variability in concentration (Figure 3d–f).

2.4. EHCGen Directional Organization

It has been shown that by enhancing the hydrophilicity of a surface, the organization and mechanical properties of collagen can be changed with surface chemistry and topography

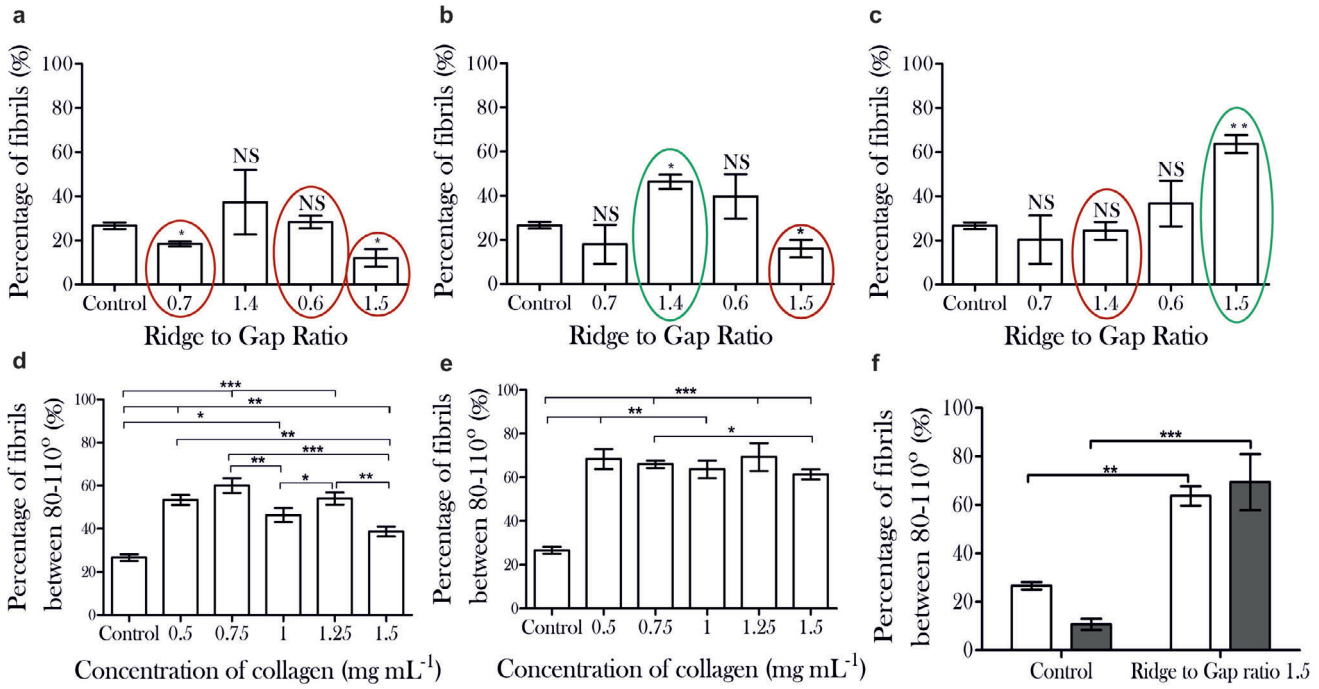

Figure 3. Quantification of percentage of fibrils aligned between 80°–110° of the ridge edge. Percentage of fibrils aligned at an average of 90° to the grating (range: 80°–110°) at structural heights of a) 200 nm, b) 500 nm, and c) 1000 nm. Red circles: collagen repeats within ± 10°of each other, green circles: statistically significant repeats versus control, i.e., a non-patterned substrate with a randomized meshwork of collagen fibrils. Alignment as a function of varying collagen concentrations on the patterned substrates with RTG ratios of d) 1.4 and e) 1.5, which was identified as an optimal average concentration of collagen deposited onto the micro-patterned yielding the highest proportion of perpendicularly assembled fibrils. f) Quantification of the percentage of fibrils aligned between 80°–110° of the ridge edge of polystyrene (white) and the PMMA (grey). ***p<0.001, **p<0.01, *p < 0.05, NS is not statically significant. n = 75 across three biological samples. Error bars refer to ± standard deviation.

determining the level of orientation and organization.[40,41] The more hydrophobic substrates yielded either collagen aggregates or large fibrils. Hydrophilic surfaces resulted in a smooth initial layer followed by a mesh-like structure of collagen at longer assembly times. This, in turn, altered the overall mechanical properties of the collagen matrix, with a more hydrophilic surface allowing for a higher mechanical stability of the collagen structure.[41] Overall, a larger amount of collagen was assembled onto hydrophobic in comparison to hydrophilic surfaces.[40,42] Since the surface chemistry can dictate the adsorption of collagen molecules and the initial organization of the self-assembly process, hydrophobic polymers (e.g., Polystyrene/PMMA) were chosen for the EHMN pattering. To verify whether the surface chemistry influenced the collagen orientation, the degree of alignment was compared between polystyrene and PMMA, with the former exhibiting a lower surface energy and being slightly less hydrophobic. Whilst no significant difference was identified between the percentage of fibrils aligned perpendicular to the ridge between the polystyrene and the PMMA, a significant difference was observed between the percentage of fibrils aligned when compared to the non-patterned control surface of each material. This indicated that the more hydrophobic underlying PMMA substrate with an average RTG of 1.5 acted as a more highly aligning substrate for collagen fibrils.

Having established the optimal assembly conditions of collagen, we have optimized the pulling speeds of the rig for controllable structuring of collagen molecules onto the EHMN patterned substrates. Initially, low pulling speed (e.g., ≤14.9 µm min^{-1}), produced inconsistent structures, which failed to achieve discreet collagen organization on the substrate.

The irregularities and merging attributed to Rayleigh instabilities did not allow for the sufficient difference in the frictional adhesion force to be achieved at the pinning or de-pinning stages of the controllable evaporative deposition process. As the rate of substrate withdrawal from the collagen solution increased (≥52.0 µm min^{-1}), discreet horizontal, dimensionally consistent (*p < 0.05) collagen patterns were generated. Further increasing the templating speed, a new hierarchical layer started to generate above the initial y-axis pulling direction with a nematic-like structure. Interestingly, an increase in templating speed initially yielded a decrease in the diameter of the collagen alignment until the speed of 96.3 µm min^{-1}, whereafter the diameter increased again at >147 µm min^{-1}. This could be explained through the theory of pinning and depinning of the three-phase contact meniscus. As the speed increases, the moving meniscal motion of the substrate through the templating solution increases the turbulent flow of collagen fibers within the solution, bringing these to the surface. The increase in the collagen at the three-phase interface allows the fibers to accumulate and bundle, possibly in a twisting motion, yielding the horizontal band, i.e., the pinning motion, which proceeds until the stepper motor moves to the next position. As the templating speed increased, the frequency of the stepper motor for each step also increased and hence, the accumulation of collagen fibers at the three-phase contact line

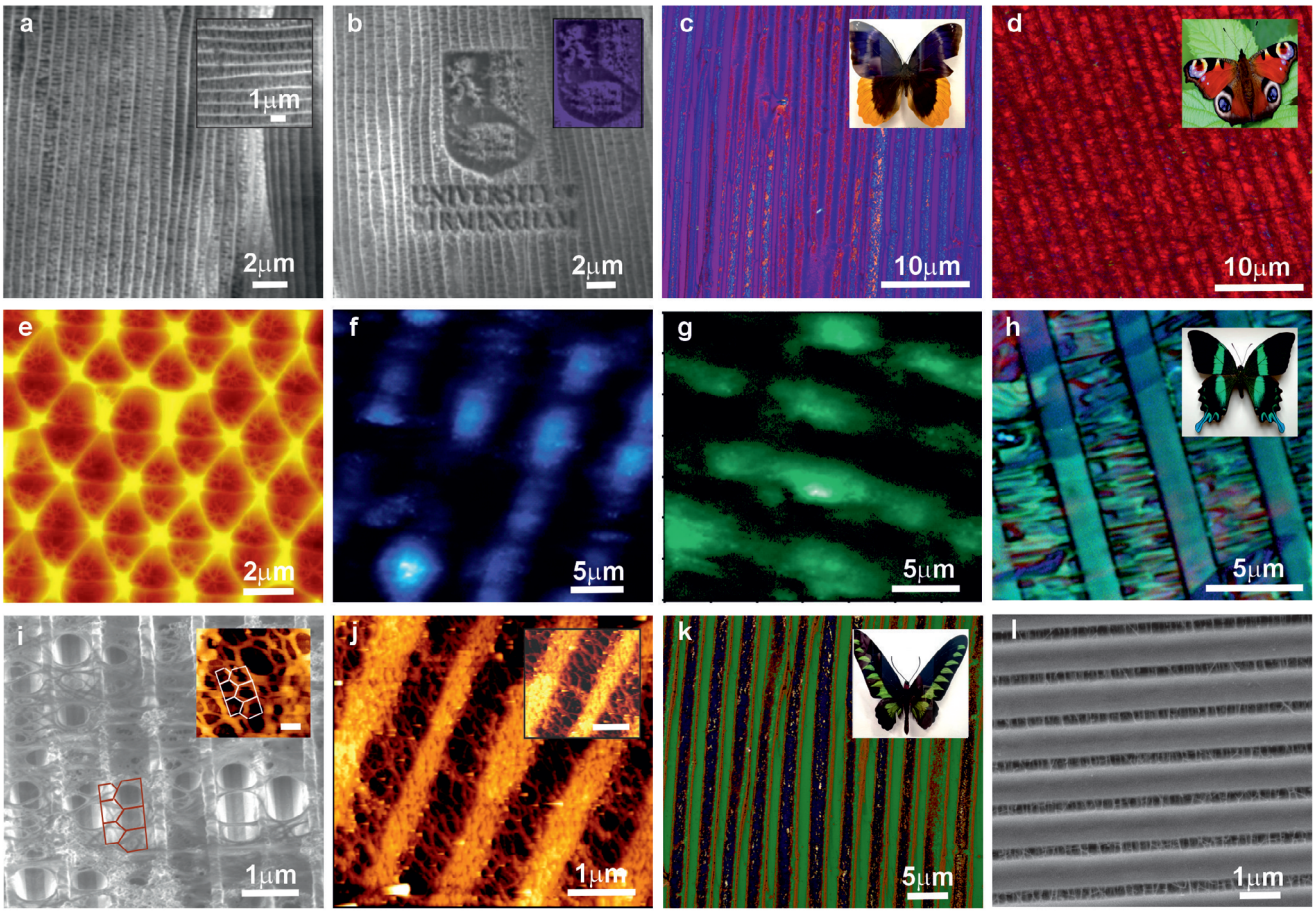

Figure 4. Representative SEM images of the a, b) EHCgen fabricated metallized substrates consisting of stacked ridges with cross-rib collagen fibers and the underlying thin film scattering longer wavelength of light (under horizontally and vertically polarized excitation illumination), exhibiting mostly purple structural colors under the perpendicular incident light c) mimicking the wings of the *C. Uranus* butterfly and red colors at skimming light incidence d) biomimicking the *Aglais io*. e) AFM height image of the artificial biomimicking collagen hierarchical micro-nanograting with transverse mode orientation of the collagen fibrils aligned horizontally across the underlying topographically EHMN structured substrate. Polarized optical microscopy images f, g) of the collagen fiber bundles assembly across the groove and ridge areas from the overall periodic array of diamond-like prisms display characteristics similar to the natural *Lycaenidae* and h) *P. Blumei* butterflies' bluish–green scales (green under the perpendicular light green and blue at skimming incidence) with the well-separated distribution of the nanostructured collagen holes providing the color and the second underlying microstructures absorbing the transmitted light and preventing it from being back-scattered, appearing turquoise under the optical microscopy. SEM and height AFM images of the EHCgen fabricated artificial replicas of an i, k) quasi-honeycomb-like structure with a j, inset) an alternate arrangement of pentagon-like irregular holes and the longitudinal parallel ridges biomimicking the *T. Brookiana* (insets) butterfly, with the latter in the l) artificially generated mimics from the inverted EHCgen patterned (non-metallized) substrates forming netlike collagen nanoholes connecting the space between the steep longitudinal ridges (seen in the zoomed-in SEM image with an average grating period of 0.9 μm), channel light into the holes and increase absorption mimicking the black areas of butterflies.

bundles over a shorter distance on the substrate, producing a narrower gap between the structures. At higher templating speeds (>147 μm min^{-1}), the increased turbulence within the collagen solution, caused by the quicker movement of the substrate, disrupted the accumulation and bundling of collagen at the three-phase contact line. This, combined with the fast-stepping motion of the motor, brought a higher concentration of collagen to the surface in the depinning motion, enabling the fibrils to further attach to the substrate between the horizontal bands. This combination of factors yields an increased gap between the structured molecules in the 3D array. The overall controllable evaporative deposition setup enables the micro-to-nanogap structuring of collagen molecules onto the underlying substrates.

Collectively, the self-assembly is the joint result of the i) lubrication provided by liquid joints (i.e., menisci), which circumvent dry friction between surfaces, ii) self-alignment arising from a combination of capillarity and geometrical shape-matching and iii) the favorable downscaling of surface tension effects with size. Structured collagen molecules on the underlying patterned substrates exhibit a different behavior relative to the bulk due to the configuration being hindered by the confinement of fibrils at the micro- and nano interfaces. When microstructured substrates are immersed in the collagen solution, there is an absence of confinement or chemical potential resulting in an initially stochastic fibril assembly. This is followed by the reduction of the free energy of collagen on the underlying physical microcues,

guiding the orientation of fibrils according to the balance of the interfacial energy (due to the interface formation) and the nonlocal molecular repulsion. The underlying patterned surface guides, the itinually randomly distributed, collagen to align perpendicular to the grooves, reducing the overall system energy imposed by the boundary conditions. In the confined geometry there is a dominance of the liquid surface, interfacial tension, and surface forces at length scales below the capillary length. Whilst the underlying substrate is being pulled at a pre-set/desired rate, the viscous forces dominate the gradual and homogeneous thinning and orientation of the collagen molecules. The evaporation leads to a loss of solvent and an increase in viscosity and density, slowing the shear and guiding the patterning of the collagen fibrils on the underlying topographical surfaces. The perpendicular alignment is a result of the decrease in elastic energy in response to the confined arrangement formed by the hybrid boundaries.[43]

2.5. EHCGen Fabricated Micro-Nanostructures

Subsequently, hierarchical 3D collagen micro-nanostructured networks were plated with noble metals via electrodeposition and plasma sputtering (Figure S6, Supporting Information), generating a range of topographic features, characterized via the low angle backscattered scanning electron microscopy (SEM), atomic force microscopy (AFM) and polarized light microscopy (POM) (Figure 4). The fabricated structures consist of several layers, forming multidimensional gratings. The first, the bottom one, is comprised of thin homogenous nanofilm resulting from the depletion process during the EHMN structure formation, where a fluid flow during the amplification of the initial capillary film undulations led to a lateral redistribution of the polymer from surrounding thinning regions. These, are further pinned to the top electrode from the surrounding polymer film by draining the liquid bridge that connects them with the unruptured polymer film. During the electrohydrodynamic grating formation, most of the patterned polymer is drawn upward toward the top electrode, resulting in redistribution of the material and thinning of the initially smooth homogenous film surrounding the rising plugs, leaving an intact smooth thin film layer once the patterning is complete. The thickness of the underlying film is controlled by the EHMN experimental parameters including the initial homogenous polymer film and the inter-electrode spacing as well as the patterning time. This, in turn, yields control over the underlying color of the thin polymer nano-film (21–1500 nm) supported on silicon, surrounding the micro-ridges. Starting from brown (≈18 nm), through blue (100–120 nm) and yellow and onto light purple (250–280 nm), pink (520 nm) and eventually to alternating light green and pink (≈1.5 µm), the color eventually changes to transparent grey for thicker films, enabling to mimic the chitin/melanin like colors in conjunction with the hierarchical structures.

Subsequently, EHMN patterned gratings with an array of ridge-like underlying sub-micron architectures (width range: 0.3–9.0 µm) and connecting the cross rib-like collagen nanostructures, perpendicular to the grooves, yielded a range of hierarchical structures (Figure 4). These comprised high longitudinal ridges with cross bars, forming open hole-like structures with average widths varying from 120 to 3 µm, overall creating multilayer with various structural colorations (Figure S5, Supporting Information). For instance, the micronano-structures with a grating of 450–900 nm, the underlying bottom smooth thin films, and collagen-formed spacing cavities generate blue and green structural colors, (Figure 4f–h) resembling the *Morpho* butterfly species. On the other hand, collagen lying transversely to the micro-ridges with cross-rib open nano cells (<210 × 300 ± 30 × 57nm>) yields violet structural colors due to the substrates forming a dense array consisting of stacked ridges and the underlying thin film scattering longer wavelength of light, exhibiting mostly purple color, seen in the upper wings of the *C. Uranus* butterfly (Figure 4a–c). These, under the perpendicular incident light and red at a skimming incidence, are representative of the *Aglais io* butterfly (Figure 4d) with an average ridge of 2 µm and holes 570 nm in width. The overall collagen intermediate holes' diameter guides the degree of reflection of light channeled into the grating ridges affecting the absorption, with an increased quasi-periodicity reducing the reflection. Low surface area and dense ridges packing of the micronano-structures in general result in a higher reflectance.

Further fabricated hierarchical assemblies, imparting structural optical properties are comprised of a multilayer architecture of micron-sized patterned diamond-like morphologies with concavities of nanostructured collagen arrays (300–2700 nm), filling the space below the open micro-ridges (Figure 4e). These, closely mimic the *Polyommatus Daphnis*, i.e., the *Lycaenidae* and *Papilio Blumei* butterflies bluish–green scale known as "pepper-pot" structures in microcells, placed between the dorsal and ventral side of the scale,[44] forming a photonic crystal-like structure. This hierarchical nanostructure, analyzed via horizontally and vertically polarized excitation illumination (Figure 4f,g) with an AFM-coupled confocal scanning microscope (indicating Raman scattering activity of the structures) reveals an interplay of polarization with the undying structural topography. Since the elastic scattering is dependent on the size of the scatterers, the microstructures have a dominant signal with the periodic array of diamond-like prisms and the additional, well-separated periodic distribution of the intermediate intensity, originating from the nanostructured collagen. The topographic surfaces comprised of alternating ridges and grooves with a range of RTGs directing the assembled collagen molecules perpendicular to the substrate and specifically registering with the underlying physical pattern via liquid crystal-like biomaterial exhibiting self-organization, phase transition, and molecular orientation, yield the photonic nanostructures. These can inhibit specific wavelengths of light guided by the underlying structural quasi-periodicity, increasing the reflection in the blue region and reducing the penetration of light into the micro-layer (Figure 4h).

Additional micro-nanostructures arranged in a mostly regular pattern oriented at the same angle to the plane with parallel longitudinal ridges spaced on average 900–1200 ± 300 nm with irregular holes distributed arbitrarily on the ridges, (Figure 4i–k) create perforating semi-periodic holes with representative multilayer structure with 1000 ± 120 nm in height and 300 ± 90 nm in width. These yield a green structural color, mimicking the *Trogonoptera Brookiana*, approximated by a quasi-honeycomb-like structure with an alternate arrangement of pentagons.

It is further possible to control the mimicking of properties of the lower side of the butterfly wing as well as the black upper-side

areas known for their unique light trapping features, producing the ultra-black effects, by creating a sparse material with high surface area to increase absorption and reduce surface reflection. This is achieved by embedding the top micronano-structured substrate in a hybrid epoxy/PMMA matrix with subsequent removal of the scaffold, releasing the inverted free-standing micro-nanoarchitectures, which are then replicated into a metal 3D-structure (Figure 2f, bottom right). These, when gold-plated, yield 3D free-standing optical elements comprised of hierarchical collagen-based assembled morphologies with netlike fine fibrils filling in the space between and connecting the steep longitudinal parallel (with an average distance of 0.81 ± 0.12 µm) ridges (Figure 4l), with inherent variation in hole shape, known to increase absorption and light-trapping effects at non-normal incidence angles.[45,46]

Given that there is no intrinsic lower limit to the EHMN patterning, the spatial resolution achievable for this lithographic method is dictated by the collagen dimensions. There is an interplay between the collagen molecules acting as nanostructuring biomaterial and the fabricated micropatterns, where the resolution required for the fabrication step of the larger-scale structures can be lesser than that of the collagen molecules. Our primary substrates have a resolution of ≈300 nm width and 90 nm depth ridges, topologically guiding the assembly of collagen, determined by the inter-structural arrangements within the generated nano-morphologies. Thus, the fundamental limit of the overall lithographic method is determined by the dimensions of the collagen, which in our case is 12 nm in diameter, and which can be tailored via the choice of collagen type used for patterning.

2.6. Optical Characteristics of the Micronano-Architectures

The fabricated micro-nanomaterials were subsequently studied for optical properties and understanding of their interaction with light via polarized light and optical birefringence microscopy. EHCGen heretical structures consist of various stacks of layers comprised of thin depleted residue nanofilm, patterned gratings, and collagen-structured molecular nanocavities, used as templates for the infiltration of symmetric gold layers separated by air gaps, yielding the optical reflection and properties (Figure S5 and Table S5.1, Supporting Information). These 3D-micronanostructured collagen-based substrates, allow for the non-local effects in the surface plasmon resonance, yielding angle-dependent color changes of the surface. With reflectance varying due to the structural motifs, gaps, and dielectric filling, the polarization with respect to the incident light yields a similar spectral shift of metamaterials.[47] The gold-plated substrates exhibited predominantly blue shift on the surface and when tilted, a strong nonlinear angle-dependent, red-shifted reflectance. The reflectance of linearly polarized light, as a function of the angle and wavelength of light at the substrates (ridges: 0.6–2.1 µm, cross-rib holes: 0.15–3.0 µm, $n = 12$), ϕ and λ, respectively in the range of 450–900 nm (**Figure 5a**) exhibited significant changes at small angles of $\phi \leq 10°$, further visible via MATLAB simulation exhibiting an average resonance-like effect from the substrates (Figure 5b). The hierarchical micro-nanostructures, at increased templating speeds, yield a more intricate system of 3D arranged collagen on the EHMN substrates, which generate optical cavities within the layers, where the incident light is trapped and slowed down whilst propagating through the structure. Reducing the refractive index of the 3D gold micro-nano patterned collagen, a metamaterial-like effect is observed for $1.5° < \phi < 6.0°$ and sub-micron underlying gratings (<900 nm) whilst for the larger ridges (>0.9 µm), similar behavior was observed at $1.7° < \phi < 4.8°$ with an overall optimal window of $2.75° < \phi < 3.25°$ achieved at high controllable evaporative deposition templating speed. This lays the platform for the possibility of controlling and considerably slowing down the incident light to such an extent that whilst the propagation direction remains constant, a negative phase velocity occurs, yielding a negative refraction angle in the structured bionano-material. Further modeling indicates that the hierarchical periodically nano-structured collagen gratings could be applicable as compatible 3D bionano metamaterials. Finite difference time domain simulations demonstrate that the coupled surface plasmon resonance from gold-plated substrates can induce optical x–y polarized light propagations. In these nanostructure arrays, the modeled effective permeability of 3D arrays around the resonant frequency exhibits a typical Drude–Lorentz feature. This lays the theoretical possibility of a negative permeability $\mu_{r,\text{eff}}$ in such elements, for small damping (Figure 5c). Light polarized in different directions couples differently to localized plasmon resonances of the ordered noble metal network at the submicron scale. The nanostructured arrays yield a reduction of the plasma frequency of gold with a decrease in reflection, explained by the Drude model in a lessening of plasma frequency from the bulk value. Thus, the composite EHMN-collagen gold could constitute a new material with distinct optical characteristics (Figure S7, Supporting Information).

A marginally undulating reflectance spectrum of the micronano-structured layers of ridges and cross-spars, with a characteristic peak at ≈450 nm exhibited 21% higher reflectance relative to the thin underlying polymer film reflector with 210 nm thickness, due to the wider spatial spread of the reflected and scattered light flux of the latter (Figure 5d). The hierarchical morphology of micronano structure with thin ridges and sparse cross-collagen holes formed a stacked array peaking in the blue wavelength region (Figure 5d, inset). The reflectance of a typical dielectric micronano-surface exhibits an average extinction band at 457 ± 21 nm, and the metallic modulated nanostructure at 480 ± 30 nm (Figure 5e). The further absorption dips arise from the resonant coupling to surface plasmon polaritons, the different directionality of the polarized light coupling to the localized plasmon resonances of the Au nanonetwork and the polarization of nano-domains relative to the incident light, yields similar spectral blue shift in metamaterials.[47] A considerably, 12–18-fold, lower reflectance (between 0.06% and 0.09%) and an enhanced absorption from resonance effects at the same wavelength, are observed for the micron-nanostructured substrates with higher surface area and deeper and wider ridges and holes. This is characteristic of the butterfly adwing-like and the black areas with increased light trapping features. Overall, smaller widths and lengths of the holes facilitate reduced reflectance with the lateral sizes having more prominent effect influences on reflectance compared with depths.[48]

Different hierarchical micronano-structures result in diverse light absorption. Holes with typical dimensions in the range of

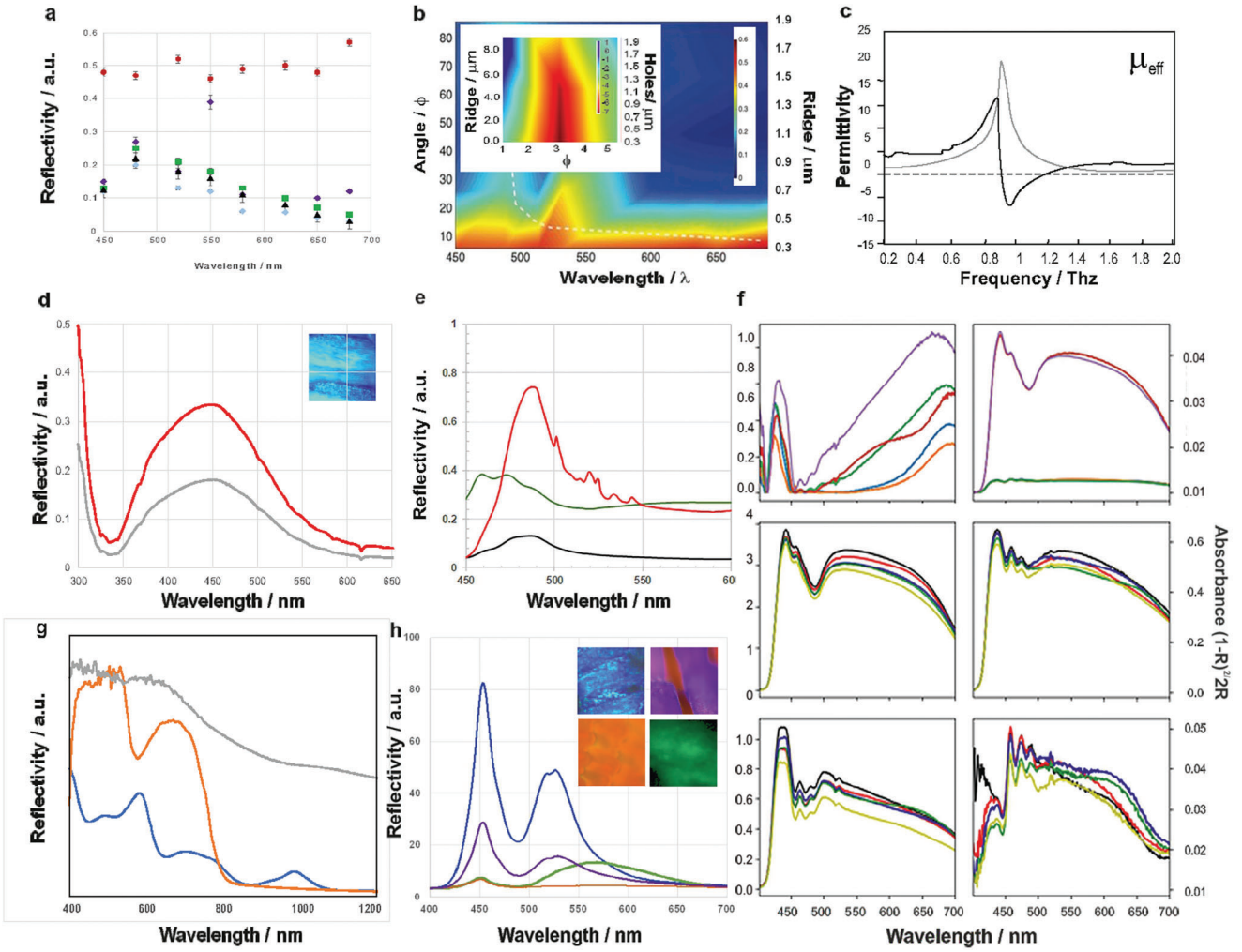

Figure 5. Angle dependence of the operation wavelength of a) reflectance versus wavelength of light directed at the substrate at angles of 86° (black triangle), 66° (green square), 46° (blue diamond), 26° (purple diamond) and 6° (red circle) and b) numerical extinction versus wavelength and angle of incidence of the substrate exhibiting significant resonance shift toward longer wavelength with a decrease of the incident angle. MATLAB mesh plot (inset) of the angle variation versus the refractive index of the EHCgen patterned arrays and the varying ridge and cross-rib diameters of collagen holes demonstrating the effect of ϕ (at $\lambda = 700$ nm) with varying refraction angles. c). Theoretical effective permeability of EHCgen gold micro- and nanostructure around the resonance frequency with FDTD of a 3D representation of gold nanonetwork. d). Reflectance spectra of the micronano-structured multilayers of ridges and cross-spars and a thin underlying polymer film reflector with 210 nm thickness with (inset) the array exhibiting blue reflection. e). Reflectance variation of a dielectric micronano-surface (green), metallic modulated nanostructure (red), and (non-metallized) micro-nanostructured substrates with higher surface area with deeper and wider ridges (black). f). Absorbance spectra for the EHCgen patterned substrates with varying sizes of 500 nm (top left), 400 nm (middle left), 300 nm (bottom left) and EHMN gratings only (500 nm (top right), 400 nm (middle right), 300 nm (bottom right)) with widths of 100 nm (black), 200 nm (red) 300 nm (blue), 400 nm (green) and 500 nm (yellow) with a significantly increased absorbance in the 420–450 nm region of the spectrum. g). The reflectance changes as a function of the variation of hole widths, reducing from the highest reflecting bare silicon substrate (gray) when the hole widths decrease from 1200 nm to below 480 nm. With the bio-mimicked structures reducing reflectance for any incident angle, the increase in the angle of incidence leads to a redshift in the extinction resonance due to the structural angle dependence whilst rotating the substrate by 180° yielding directional green to bluish reflection with underlying flat blue-reflecting thin film in the longer wavelength range. h). Reflection spectra for unpolarized incident light of hierarchical gold-infiltrated collagen-EHMN micro- and nano-morphologies with the characteristic peaks and reflection of blue, green, purple, and orange (inset) optical responses as a function of the structural dimensions.

hundreds of nanometers, significantly alternating the interactions with incident light and the arrays of underlying diffraction EHMN gratings with perpendicular slits on the magnitude of λ,[49] yield efficient optical diffusers in the visible range. Whereas the quasi-honeycomb-like structures, diffract the incident light into the grooves to be absorbed. These exhibit the reflectivity peak at 450 nm with the highest reflectance found in the blue region (>80%) and considerably decreased values in the green/orange spectral ranges (<10%) (Figure 5f,g). It is overall observed that the layers of quasi-periodic holes between ridges with increasing spacing up to >1.2 μm, resulted in higher reflectance, considerably dropping for the hole widths decreasing below 480 nm (Figure 5g). Controlling the deposition of the collagen-formed nano-holes, particularly within the wavelength range of visible

light, enables achieving enhanced absorption from localized plasmon resonance effects when the hole radius is roughly proportional to the wavelength of light[50] with for instance, orange and red peaks absorption at ≈480 and ≈520 nm, respectively (Figure 5f). The absorption peak of gold EHCgen patterned substrates is on average more than three times higher than the non-structured counterparts, indicative of the enhancement of optical absorption caused by the 3D micronano-architectures. The electric field amplitude of localized surface plasmons is 3.9-fold enhanced due to the coupling with the 3D architectures relative to the non-structured surfaces. With the bottom nanofilm guiding most of the light to propagate through the holes, it is repeatedly reflected by the oblique ridge walls, leading to the augmentation of the effective path length for light absorption, resulting in multiple reflections. The elaborate 3D quasi-honeycomb hierarchical micro- and nanoarchitecture that does benefit the near-infrared light harvesting amplifies the response of Au to light with the absorption peak reaching almost twice that of non-structured counterparts, indicating an enhancement of optical absorption caused by the 3D EHCgen architectures. The deep vertical ridges with little or no holes show the highest visible light absorption (≈70%) and collagen-generated holes appear to reduce the absorption abilities as a function of the decreased number of lines of holes (from typically three to one) between the ridges.

For the micro-nanostructured periodic array of diamond-like prisms the generated cavity resonances for light reflected off the interstitial regions between adjacent incurvatures result in subtle color hue variations whereas, for the thicker concavities, the surface resonances are closely spaced in wavelength compared to the interstitial regions. A redshift in the reflectance spectra is observed as the interstitial gap space becomes larger, confirming the dependence of the optical response of the structure on the gap distance/diameter. The dependence on illumination polarization (0° indicating the position where the sample is parallel to the polarization of the incoming light with reference to mirror and parallel polarizers, rotating the surfaces between 0°, 90°, and 180°) indicates that larger electromagnetic fields are localized in the interstitial space between adjacent microstructures. While incident radiation excites a plasmon trapped in this interstitial space, the polarization charges on either side of the gap oppose each other. This produces high dipolar coupling fields, resulting in interstitial plasmons. At the non-normal incident light, turning the thickness of the polymer film and the cavity leads to the variation of the resonant light transmitted through the top layer, modifying the retro-reflected observed hue from the pronounced green to bluish at skimming incidence (Figure 5g).

When an incident light interacts with the hierarchical gold-infiltrated collagen-EHMN micronano morphologies, it partly passes through the open nanoholes, reaching the underlying ridges and the thin residue nanofilm, reflecting various colors in the visible range (Figure 5h). These depend on the micronano morphology dimensions with the lateral bands' width arising from the ridge arrays acting as gratings.[51,52] The reflected light subsequently, exits through the open cross-ribs, resulting in a blue-colored band, or scattered by the structures and the thin film reflector, resulting in a sparse blueish scattering color band. Furthermore, parts of the incident light hit the grid of ridges and are partly reflected by the slightly overlapping hierarchical architectures. These act as an array of multilayers consisting of a layer of high refractive index material, on the order of hundreds of nanometers in thickness, surrounded by air, resulting in an additional blue–green peak, spatially shifted to the longer wavelengths. The primary maximum extinction band is observed ≈450 nm and a minimum at 500 nm (an underlying film of 150 nm yielding the red–purple colors (Figure 5h, inset)) with a further maximum progressively red-shifting λ contribution to the reflectance in the longer wavelength range. These yield broader peaks for the vertically oriented ridges at 525 and 570 nm (and underlying film with a thickness of 210 nm), resulting in the overall purple–blue and green reflected colors, respectively.[53,54] This is due to the variation of the plasma frequency by the nanostructuring and corresponding air fraction,[55] where the gold-surface plasmon has been shown to shift to <500 nm with comparable extinction at 520 nm, previously observed for nanoparticles. This is in correspondence with the Au nano rod-like structures, where the short-wavelength transverse mode matches the gold nanoparticles and the long-wavelength longitudinal mode, produced by the optical field along the rod-like nanostructure.[47]

3. Conclusion

Herein, a novel hybrid bottom–up and top–down bionano lithographic process for hierarchical 3D micronano-architectures has been developed via guided assembly of collagen building blocks as templating intermediates combined with a hybrid electrohydrodynamic micro-nanopatterning. This enables generating a range of quasi-ordered mimics of photonic crystal-like metamaterials. Engineering of new structured materials and properties via biosynthetic biology origin enables a route of exploiting collagen molecular constituents' capacity as "Lego" blocks to self-assemble into diverse hierarchical micro-nanostructures. Being unavailable by conventional lithography or wet nanochemistry techniques, this further allows control over the dimensionality of the evolving 3D architectures. The facile collagen-based lithographic technique provides the ability for a straightforward design, manufacture, and control of robust submicron patterns at low cost and high throughput. Patterns' resolution ranging from nanometer to micrometer scale precision, can be fine-tuned via adjustments of the physical and experimental parameters including the nanofilm thickness, collagen's pH and concentration, assembly time, speed of patterning, and the selection of the underlying guiding substrate. Its versatility and application appeal are emphasized by the possibility of patterning a wide range of underlying materials combined with single and multilayer biomolecular assemblies. This yields a variety of hierarchical architectures and anisotropic sub-structures and with the inherent compatibility with aqueous conditions, renders it particularly conducive to patterning biomolecules. Therefore, the inclusion of this lithographic route into the established manufacturing processes is envisioned.

The fabricated 3D EHCgen architectures were subsequently studied for optical properties and understanding of their interaction with light and the optical response of the novel assemblies assessed via extinction and reflection measurements of the left- and right-handed circularly polarized light. The hierarchical architectures characterized by hole and ridge arrays with different sizes and arrangements, creating surfaces with interesting optical properties, have been found to exhibit a range of

visible colors. For instance, iridescence-like color is observed, when spot-illuminated with white light, or opposite optical responses, when analyzed by polarized microscopy and reflectance measurements. This demonstrated that size-and-orientation-dependent nanofilaments with varying degrees of lateral order yield distinctly colored structures correlating with the characteristic spectra. For the steeper ridges and larger holes, increasing the surface area for absorption within their structure, the incident photons are found to be largely absorbed with an absorption peak arising from the resonance between holes and the incident light. Further classical electrodynamics calculations, considering the full multipolar response of the fabricated metamaterials via a multiple scattering formalism, revealed the presence of an ordered and continuous nanometer-scale network. This yielding a reduction of plasma frequency of the noble metal plated material with the polarization-sensitive anisotropic localization could enable further a possibility of switchable nanophotonic logic devices and multiplexed detection at the single structure level. Whilst the underlying nano-films, acting as thin reflectors, can exclusively yield the coloration, a more intense reflection is observed when the micro-ridges form tall stack-like structures. These act as reflective multilayers, where increasing the number and decreasing the distance between them enhances the obtainable reflectance and brightness.

Further to acting as novel free-standing micro- and nano morphologies, it is possible to exploit the fabricated EHCgen platforms for tailor-designing and engineering a virtually unlimited range of micronano network structured morphologies and from materials of choice, e.g., alloys, ceramics, or perovskites, to create novel properties and optical performance. Moreover, since in solution, collagen fibers can interact with a range of constituents including nanomaterials, carbon-based materials, nanoparticles, quantum dots, and buckyballs to produce complex ordered structures, the thought-after patterned substrates can be prefabricated to have specific functionality. These can be then transferred into the continuous nanonetworks, incorporated with functional materials to interconnect with 3D scaffolds. Such functional network bionano materials, exhibiting an increased performance due to the high aspect ratio and nanoscale features, will lay the platform for a range of potential uses including photovoltaics, optical imaging, electrochemical and light-storage devices, cloaking materials, high-speed optical computers, and nano-lasers as well as numerous further applications in transformation optics.

4. Experimental Section

Materials: Solvents (ethanol, toluene, and methanol) were purchased from Sigma–Aldrich and Fisher Scientific. Polystyrene 100 kg mol^{-1} was for the EHMN lithography (Polymer Standards). Materials were used as received with no further purification steps. Highly polished *p*-doped silicon wafers with <100> crystal orientation (Wafernet) were used during the EHMN as bottom and top electrodes (X-lith eXtreme Lithography). Four species of butterflies (*Trogonoptera Brookiana* male, *Morpho Dididus*, *Danaus Plexppus*, and *Caligo Uranus, male (Gold Edged Owl)*), were acquired from commercial suppliers (Durham, USA, Minibeast, UK). All specimens were kept mounted in wooden insect boxes with naphthalene to prevent decay between measurements.

EHMN Micronanopatterning: Polystyrene and N-acetylglucosamine polymers were used for thin film deposition and patterning during the EHMN patterning and highly polished *p*-doped silicon wafers were used as electrodes in the capacitor set-up. Silicon wafers were cleaned in a "Piranha" solution of 3:1 sulfuric acid and hydrogen peroxide, followed by rinsing with deionized water and drying under nitrogen. An initial solution of polystyrene in toluene 3%w/w was spin-coated onto the freshly cleaned 1.0 × 1.0 cm^2 electrodes and these were electrically connected to the external voltage supply and annealed above the polymer's glass transition temperature. The EHMN patterning capacitor was enclosed inside a high-precision performance convection oven, where the temperature was thermostatically controlled, ensuring that there was no temperature gradient on the substrates. Once the EHMN process had been completed, the capacitor set-up was cooled down to RT to quench the formed structures, and the external voltage supply was disconnected.

EHCgen Lithography: A dedicated rig was designed and engineered for an evaporative deposition with an automated micrometer-based withdrawal system controlled through a Raspberry Pi and configured with a Gertbot GUI, allowing drawing speeds in the range: 01.48–148.60 mm min^{-1}. The integrated micrometer allowed for micro-adjustments of the speed within a few microns. The withdrawal rates of the stepper motor were calculated as follows: For ECD, 8 mL of the templating collagen solution contained within a 10 mL beaker was used to maintain the same basal conditions of the meniscus at the three-phase contact line. A range of collagen solutions were prepared at concentrations of 0.5–5 mg mL^{-1} and subjected to ECD on EHD-patterned substrates at a selected speed. The step angle of the stepper motor was 1.8° and 360° represented a 500 µm withdrawal distance, therefore a full 1000 µm withdrawal distance equal to two full 360° rotations of the micrometer: 360°/1.8° = 200 steps per rotation. The frequency of steps per second was inputted into the Gertbot GUI, e.g., for a frequency of 1F to travel 1000 µm, 403.95 s mm^{-1} = 0.40395 s mm^{-1} = 148.533 µm min^{-1}. Conversion calculated for withdrawal feed rates as F values inputted into the Gerbot GUI are summarized below. The resulting micro-nanostructures were gold-plated via electrodeposition and sputtering with an initial nucleation step of 0.0 and −1.2 V and a 50 mV s^{-1} at scan rate followed by the deposition step of 3 s at −0.8 V. The nanostructures were alternatively coated with a thin gold nanofilm using an Emitech sputter-coater with a direct current argon plasma (Au of 99.999% purity, Kurt J. Lesker) using two cycles of 10 s at 70 mA. To fabricate the inverse ECHGen morphologies, collagen-EHMN gratings were embedded in a hybrid epoxy/PMMA matrices with subsequent removal of the scaffold, releasing the inverted free-standing micro-nanoarchitectures, which were then replicated into a metalized inverted 3D-structure.

Frequency / F	Withdrawal Feed Rate / µm min^{-1}
1.000	148.533
0.750	111.400
0.500	074.267
0.400	059.413
0.300	044.560
0.250	037.133
0.125	018.567

Scanning Electron Microscopy: Small sections from the wings of butterflies *Trogonoptera Brookiana* male, *Morpho Dididus*, *Danaus Plexppus*, and *Caligo Uranus* were mounted on SEM stubs and subsequently, scanning electron microscopy (SEM) characterization was performed using a LEO ULTRA 55 SEM including a Schottky emitter (ZrO/W cathode) and a thermally assisted field emission source scanning electron microscope (FEI Helios dual beam) at acceleration voltages of 1–10 kV with a lateral resolution of 2–5 nm.

Transmission Electron Microscopy: Samples were analyzed using an FEI Technai 12 transmission electron microscope at an acceleration voltage of 120 kV. For cross-sectional imaging, a thin layer of platinum was sputter-coated on the substrate, followed by embedding in a Spurr epoxy resin. The

substrate was removed, and the remaining structure was sectioned using a diamond knife via the Leica Ultra-cut Microtome, yielding sections with an average thickness of 30–60 nm.

Finite-Difference Time-Domain and Numerical Simulations: 2D simulations of the optical response of the structures were conducted by finite-difference time-domain (FDTD) solutions consisting of regions, with structural dimensions extracted from SEM images, with boundary conditions for the simulation model of perfectly matched layer in z direction, periodic in x–y direction, auto non-uniform mesh accuracy $x = dy = dz = 1$ nm, plane wave light source, polarizes along x–y direction, $\lambda = 300$–1200 nm, frequency-domain field and power. The refractive index was estimated as $1.56 + 0.06i$ irrespective of λ and dielectric Au constant from Ref. [56,57] Absorbance of the system assumed to be equal to 1-transmissivity-reflectivity, calculated via the Kubelka–Munk function R_∞, where $R_\infty = k/s = (1-R_\infty)^2/(2R_\infty)$, where k and s are the absorption and scattering coefficients, respectively and R_∞ = measured/reference values.

Atomic Force Microscopy: JPK NanoWizard II atomic force microscope was used to characterize the micro- and nanostructures topography. The atomic force microscopy (AFM) measurements were performed using tapping mode via intermittent contact of the tip with the sample in ambient conditions. NCHV-A cantilevers with a resonance frequency of 320 kHz and stiffness of 42 N m^{-1} were used. Height and phase images were analyzed with Gwyddion's software (Version 2.55). Each scan was performed at 1024 × 1024 pixel quality at 3s/line raster rate, for a total of 1 h per region. AFM-coupled confocal scanning microscope using the NT-MDT VIT_P cantilevers was employed to study the Raman scattering activity of the structures.

Optical Characterization: A Leica DM2000 optical polarizing microscope was used to investigate the optical properties of the samples. The optical transmission and reflection characterization of the samples was evaluated in terms of variations in the intensity of light using unpolarized incident light and the attached spectrometer (Horiba). Additionally, spectral reflectance measurements were carried out with an Olympus BX51 microscope equipped with both an incoherent white light (halogen) source and a Xenon UV–vis light source (PX-2 Ocean Optics) and an optical fiber reflectance probe coupled to a QE65000 Ocean Optics spectrometer. The measurements were acquired from three to nine locations on each sample. The microscope Xenon lamp acted as an illumination source for the spectroscopic measurements. 20–100 µm optical fibers (ThorLabs) in the focal plane of the 20× objective working distance have served as a pinhole for the signal collection. Motorized MicroHR Imaging Spectrometer with solid-state UV-coated silicon over indium gallium arsenide detector for 200–1700 nm and the SynerJY for Windows software were used for data acquisition and analysis. Achromatic polarizers were used for polarization measurements. For transmission/reflection measurements in different directions, the sample was mounted on a multirotational stage enabling both the rotation around the focal axis of the objective and tilting away from normal incidence.

Supporting Information

Supporting Information is available from the Wiley Online Library or from the author.

Acknowledgements

The authors acknowledge funding from the Wellcome Trust (Grant No. 174ISSFPP) and the Engineering and Physical Science Research Council (Grant Refs.: EP/V029983/1, EP/L016346/1). The authors also acknowledge the funding from UKRI under the UK Government's Horizon Europe Funding Guarantee (ERC Consolidator Grant, EP/Y030206/1).

Conflict of Interest

The authors declare no conflict of interest.

Data Availability Statement

The data that support the findings of this study are available from the corresponding author upon reasonable request.

Keywords

biomimetics, collagen patterning, electrohydrodynamic hierarchical lithography, photonic micro-nanomaterials

Received: March 31, 2024
Revised: May 27, 2024
Published online:

[1] S. Kinoshita, S. Yoshioka, *ChemPhysChem* **2005**, *6*, 1442.
[2] W.-G. Bae, H. N. Kim, D. Kim, S.-H. Park, H. E. Jeong, K.-Y. Suh, *Adv. Mater.* **2014**, *26*, 675.
[3] O. Sato, S. Kubo, Z.-Z. Gu, *Acc. Chem. Res.* **2009**, *42*, 1.
[4] A. L. Davis, H. F. Nijhout, S. Johnsen, *Nat. Commun.* **2020**, *11*, 1294.
[5] R. Yan, M. Chen, H. Zhou, T. Liu, X. Tang, K. Zhang, H. Zhu, J. Ye, D. Zhang, T. Fan, *Sci. Rep.* **2016**, *6*, 20001.
[6] K. Yu, S. Lou, J. Ding, D. Zhang, Q. Guo, T. Fan, *Soft Matter* **2013**, *9*, 2614.
[7] Y. Xia, G. M. Whitesides, *Annu. Rev. Mater. Sci.* **1998**, *28*, 153.
[8] F. A. Boroumand, P. W. Fry, D. G. Lidzey, *Nano Lett.* **2005**, *5*, 67.
[9] B. H. Cumpston, S. P. Ananthavel, S. Barlow, D. L. Dyer, J. E. Ehrlich, L. L. Erskine, A. A. Heikal, S. M. Kuebler, I.-Y. S. Lee, D. McCord-Maughon, J. Qin, H. Röckel, M. Rumi, X.-L. Wu, S. R. Marder, J. W. Perry, *Nature* **1999**, *398*, 51.
[10] J. Joo, B. Y. Chow, J. M. Jacobson, *Nano Lett.* **2006**, *6*, 2021.
[11] J. Melngailis, A. A. Mondelli, I. L. Berry III, R. Mohondro, *J. Vac. Sci. Technol. B* **1998**, *16*, 927.
[12] Y. Xia, G. M. Whitesides, *Angew Chem Int Ed Engl* **1998**, *37*, 550.
[13] Z. Liu, J. Qiao, Z. Niu, Q. Wang, *Chem. Soc. Rev.* **2012**, *41*, 6178.
[14] P. Passaretti, Z. Schofield, J. J. S. Rickard, H. White, S. Mahajan, P. Goldberg Oppenheimer, *Adv. Opt. Mater.* **2022**, *10*, 2102784.
[15] C. K. Revell, O. E. Jensen, T. Shearer, Y. Lu, D. F. Holmes, K. E. Kadler, *Matrix Biol. Plus* **2021**, *12*, 100079.
[16] E. G. Canty, K. E. Kadler, *J. Cell Sci.* **2005**, *118*, 1341.
[17] E. G. Canty, Y. Lu, R. S. Meadows, M. K. Shaw, D. F. Holmes, K. E. Kadler, *J. Cell Biol.* **2004**, *165*, 553.
[18] P. C. Fratzl, *Structure and Mechanics*, (Ed. P. Fratzl) Springer, Boston, MA, USA **2008**, pp. 1–13.
[19] K. E. Kadler, C. Baldock, J. Bella, R. P. Boot-Handford, *J. Cell Sci.* **2007**, *120*, 1955.
[20] G. Birdi-Chouhan, R. M. Shelton, J. Bowen, P. Goldberg-Oppenheimer, S. J. Page, J. V. Hanna, A. Peacock, A. J. Wright, L. M. Grover, *RSC Adv.* **2016**, *6*, 99809.
[21] A. J. Holder, N. Badiei, K. Hawkins, C. Wright, P. R. Williams, D. J. Curtis, *Soft Matter* **2018**, *14*, 574.
[22] M. S. Sridhar, *Indian J. Ophthalmol.* **2018**, *66*, 190.
[23] E. M. McCarthy, H. Floyd, O. Addison, Z. J. Zhang, P. G. Oppenheimer, L. M. Grover, *ACS Omega* **2018**, *3*, 10129.
[24] P. Muangsanit, A. Day, S. Dimiou, A. F. Ataç, C. Kayal, H. Park, S. N. Nazhat, J. B. Phillips, *J. Neural Eng.* **2020**, *17*, 046036.
[25] U. N. G. Wudebwe, A. Bannerman, P. Goldberg-Oppenheimer, J. Z. Paxton, R. L. Williams, L. M. Grover, *Philos Trans R Soc Lond B Biol Sci* **2015**, *370*, 20140200.
[26] X. Yu, C. Tang, S. Xiong, Q. Yuan, Z. Gu, Z. Li, Y. Hu, *Curr. Org. Chem.* **2016**, *20*, 1797.
[27] C. Busà, J. J. S. Rickard, E. Chun, Y. Chong, V. Navaratnam, P. Goldberg Oppenheimer, *Nanoscale* **2017**, *9*, 1625 .

[28] P. Goldberg-Oppenheimer, T. Hutter, B. Chen, J. Robertson, S. Hofmann, S. Mahajan, *J. Phys. Chem. Lett.* **2012**, *3*, 3486.
[29] P. Goldberg-Oppenheimer, S. Mahajan, U. Steiner, *Adv. Mater.* **2012**, *24*, OP175.
[30] P. Goldberg-Oppenheimer, U. Steiner, *Small* **2010**, *6*, 1248.
[31] P. Oppenheimer, *Electrohydrodynamic Patterning of Functional Materials*, Springer, Berlin, Germany **2013**, pp. 63–78.
[32] J. J. Rickard, I. Farrer, P. G. Oppenheimer, *ACS Nano* **2016**, *10*, 3865.
[33] K. E. Kadler, D. F. Holmes, J. A. Trotter, J. A. Chapman, *Biochem. J.* **1996**, *316*, 1.
[34] Y. Li, A. Asadi, M. R. Monroe, E. P. Douglas, *Mater. Sci. Eng., C* **2009**, *29*, 1643.
[35] S. Nihon, Y. T. Nagai, Y.T Japanese Biochemical Society, *J. Biochem.* **1973**, *74*, 253.
[36] M. Achilli, D. Mantovani, *Polymers* **2010**, *2*, 664.
[37] E. M. McCarthy, *The External Manipulation of Collagen Type I Using Inorganic Ions and Topographical Cues*, University of Birmingham, Birmingham, UK **2019**.
[38] J. R. Harris, A. Soliakov, R. J. Lewis, *Micron* **2013**, *49*, 60.
[39] J. Glass-Brudzinski, D. Perizzolo, D. M. Brunette, *J. Biomed. Mater. Res.* **2002**, *61*, 608.
[40] F. A. Denis, P. Hanarp, D. S. Sutherland, J. Gold, C. Mustin, P. G. Rouxhet, Y. F. Dufrêne, *Langmuir* **2002**, *18*, 819.
[41] E. Pamuła, V. De Cupere, Y. F. Dufrêne, P. G. Rouxhet, *J. Colloid Interface Sci.* **2004**, *271*, 80.
[42] F. A. Denis, A. Pallandre, B. Nysten, A. M. Jonas, C. C. Dupont-Gillain, *Small* **2005**, *1*, 984.
[43] W.-J. Chung, J.-W. Oh, K. Kwak, B. Y. Lee, J. Meyer, E. Wang, A. Hexemer, S.-W. Lee, *Nature* **2011**, *19*, 364.
[44] Z. Bálint, Z. Vertesy, K. Kertész, L. Biro, Scanning Electron Microscopic Investigations in Butterfly Wings: Detecting Scale Micro-and Nanomorphology and Understanding their Functions. **2004**.
[45] W. Wang, W. Zhang, X. Fang, Y. Huang, Q. Liu, M. Bai, D. Zhang, *Opt. Lett.* **2014**, *39*, 4208.
[46] Q. Zhao, T. Fan, J. Ding, D. Zhang, Q. Guo, M. Kamada, *Carbon* **2011**, *49*, 877.
[47] S. Vignolini, N. A. Yufa, P. S. Cunha, S. Guldin, I. Rushkin, M. Stefik, K. Hur, U. Wiesner, J. J. Baumberg, U. Steiner, *Adv. Mater.* **2012**, *24*, Op23.
[48] T. K. Chong, J. Wilson, S. Mokkapati, K. R. Catchpole, *J. Opt.* **2012**, *14*, 024012.
[49] A. L. Ingram, A. R. Parker, *Philos. Trans. R Soc. Lond. B Biol. Sci.* **2008**, *363*, 2465.
[50] Q. Zhao, X. Guo, T. Fan, J. Ding, D. Zhang, Q. Guo, *Soft Matter* **2011**, *7*, 11433.
[51] D. G. Stavenga, H. L. Leertouwer, B. D. Wilts, *J. Exp. Biol.* **2014**, *217*, 2171.
[52] S. Yoshioka, S. Kinoshita, *Proc. Biol. Sci.* **2004**, *271*, 581.
[53] C. Banbury, J. J. S. Rickard, S. Mahajan, P. Goldberg Oppenheimer, *ACS Appl. Mater. Interfaces* **2019**, *11*, 14437.
[54] W.-J. Chung, J.-W. Oh, K. Kwak, B. Y. Lee, J. Meyer, E. Wang, A. Hexemer, S.-W. Lee, *Nature* **2011**, *478*, 364.
[55] J. A. Dolan, M. Saba, R. Dehmel, I. Gunkel, Y. Gu, U. Wiesner, O. Hess, T. D. Wilkinson, J. J. Baumberg, U. Steiner, B. D. Wilts, *ACS Photonics* **2016**, *3*, 1888.
[56] Z. Zhao, Z. Li, Z. Zou, *Phys. Chem. Chem. Phys.* **2011**, *13*, 4746.
[57] E. Van Hooijdonk, C. Vandenbem, S. Berthier, J. P. Vigneron, *Opt. Express* **2012**, *20*, 22001.

